Predicting human blood viscosity in silico

Dmitry A. Fedosov[a,b], Wenxiao Pan[b,c], Bruce Caswell[b], Gerhard Gompper[a], and George E. Karniadakis[b,1]

[a]Institute of Complex Systems and Institute for Advanced Simulation, Forschungszentrum Jülich, 52425 Jülich, Germany; [b]Division of Applied Mathematics, Brown University, Providence, RI 02912; and [c]Pacific Northwest National Laboratory, Richland, WA 99352

Edited by Charles S. Peskin, New York University, and approved June 13, 2011 (received for review January 24, 2011)

The viscosity of blood has long been used as an indicator in the understanding and treatment of disease, and the advent of modern viscometers allows its measurement with ever-improving clinical convenience. However, these advances have not been matched by theoretical developments that can yield a quantitative understanding of blood's microrheology and its possible connection to relevant biomolecules (e.g., fibrinogen). Using coarse-grained molecular dynamics and two different red blood cell models, we accurately predict the dependence of blood viscosity on shear rate and hematocrit. We explicitly represent cell–cell interactions and identify the types and sizes of reversible rouleaux structures that yield a tremendous increase of blood viscosity at low shear rates. We also present the first quantitative estimates of the magnitude of adhesive forces between red cells. In addition, our simulations support the hypothesis, previously deduced from experiments, of yield stress as an indicator of cell aggregation. This non-Newtonian behavior is analyzed and related to the suspension's microstructure, deformation, and dynamics of single red blood cells. The most complex cell dynamics occurs in the intermediate shear rate regime, where individual cells experience severe deformation and transient folded conformations. The generality of these cell models together with single-cell measurements points to the future prediction of blood-viscosity anomalies and the corresponding microstructures associated with various diseases (e.g., malaria, AIDS, and diabetes mellitus). The models can easily be adapted to tune the properties of a much wider class of complex fluids including capsule and vesicle suspensions.

blood rheology | blood modeling | shear thinning | aggregation force | dissipative particle dynamics

Rheological and material properties of cell, capsule, and vesicle suspensions have many applications in medicine, biology, engineering, and materials science. One of the main examples of such suspensions is blood, which consists of RBCs, predominant by volume, and a small fraction of other cells and proteins suspended in the plasma. Understanding blood flow and its relation to cellular properties and interactions may lead to advances in biomedical applications (e.g., drug delivery, blood substitutes). Moreover, a change in blood rheological and flow properties is often associated with hematological diseases or disorders (e.g., sickle-cell anemia, malaria), and therefore the viscosity of blood has long been used as an indicator in the understanding and treatment of disease.

Modern rheometry techniques and instruments yield reliable measurements of macroscopic properties of cell suspensions with ever-improving convenience—for example, the bulk properties of blood measured in various laboratories (1–6). Virtually all blood-viscosity measurements are necessarily in vitro, and before newly drawn blood is introduced into a viscometer it must at least be stabilized with an anticoagulant, which is then called "whole blood." Under flow conditions at small deformation rates, the RBCs in whole blood have been observed to aggregate into structures called "rouleaux," which resemble stacks of coins (1, 7–9). The aggregation process appears to be strongly correlated to the presence of the plasma proteins (7, 9). Experiments with washed RBCs resuspended in pure saline, to which fibrinogen was added progressively (7), showed a tremendous viscosity increase at low deformation rates with respect to fibrinogen concentration. In addition, such suspensions exhibit a yield stress (1, 10, 11)—i.e., a threshold stress for flow to begin.

However, these advances have not been accompanied by theoretical developments that can yield quantitative predictions of rheological and flow properties of blood. Recent theoretical and numerical studies focused mostly on the behavior of a single RBC in various flows (12–16). Several studies have been performed to simulate a suspension of multiple cells (16–19) in tube flow. So far, the connection between the rheology of a cell suspension and its microscopic properties on a single-cell level, such as structure or arrangement, cell viscoelastic properties, and local dynamics, is not well understood. In addition, cell suspensions are often further complicated by intrinsic cell interactions (e.g., RBC aggregation; refs. 1, 7–9). In this paper, we will establish such a link between bulk properties and microstructure, and will focus on the *quantitative* prediction of rheological properties and dynamics of blood flow by employing multiscale modeling of interacting red blood cells.

Results and Discussion

We consider suspensions of RBCs to mimic the experimental set up of washed RBCs suspended in pure saline, to which fibrinogen was added progressively (7), and we will refer to them as erythrocyte suspensions (ES). We simulate them with dissipative particle dynamics (DPD), a coarse-grained version of molecular dynamics suited to the seamless modeling of liquids and soft matter (14, 20, 21). Two different cell models are employed. The first, a multiscale RBC model (MS-RBC) (15) represents the RBC membrane with a few hundred DPD particles connected by viscoelastic springs into a triangular network in combination with out-of-plane elastic bending resistance, similar to the mesoscopic model in Refs. 12, 18, and 22. The characteristic biconcave RBC shape is achieved by imposition of constraints for constant membrane area and constant cell volume. Fitting of the model parameters is performed through a number of static and dynamic experiments on single real RBCs (15) and no further adjustment is made for the RBCs in suspension. Because simulations with MS-RBC are computationally expensive, we also employ a low-dimensional model (LD-RBC) of an RBC (23) for efficiency in parametric studies. LD-RBC is constructed as a closed torus-like ring of only 10 large hard colloidal particles, see *Methods* for more details. LD-RBC allows exploration of simulated blood flows over a wide range of hematocrits at computational costs considerably below those for their multiscale counterparts. In addition to the LD-RBC and MS-RBC models, we developed an aggregation model to reproduce the reversible rouleaux formation and destruction, which is essential to capture blood flow behavior, especially at low shear rates. Next, we present results for the ES viscosity with

Author contributions: D.A.F., W.P., B.C., G.G., and G.E.K. designed research; D.A.F. and W.P. performed research; D.A.F carried out multiscale RBC simulations; W.P. carried out low-dimensional RBC simulations; D.A.F. and W.P. analyzed data; D.A.F., W.P., B.C., G.G., and G.E.K. wrote the paper.

The authors declare no conflict of interest.

This article is a PNAS Direct Submission.

[1]To whom correspondence should be addressed. E-mail: george_karniadakis@brown.edu.

This article contains supporting information online at www.pnas.org/lookup/suppl/doi:10.1073/pnas.1101210108/-/DCSupplemental.

and without aggregation, rouleaux formation and magnitude of aggregation forces, yield stress, and the micro-to-macro link in ES.

In Silico Versus in Vitro Blood Viscosity. The experimental bulk viscosities of well-prepared nonaggregating ES and of whole blood were measured for various hematocrit values (H) at physiological temperature 37 °C in refs. 1–3. The blood viscosity in our work was derived from simulations of plane Couette flow using the Lees–Edwards periodic boundary conditions for both the MS-RBC and the LD-RBC suspensions. The shear rate and the cell density in our simulations were verified to be spatially uniform on average over time, and the viscosities were computed, with and without aggregation, as functions of the shear rate over the range 0.005–1,000.0 s^{-1} (this corresponds to the range of dimensionless shear rate or capillary number $\eta\dot{\gamma}D/Y$ between 2.5×10^{-6} and 0.5, where η is the solvent viscosity, D is the RBC diameter, and Y is the membrane Young's modulus). Fig. 1*A* shows the relative viscosity (RBC suspension viscosity normalized by the viscosity of the suspending media) against shear rate at hematocrit $H = 45\%$. The MS-RBC model predictions are in excellent agreement with the blood viscosities measured in three different laboratories (1–3). The ES model, consisting only of RBCs in suspension, clearly captures the effect of aggregation on the viscosity at low shear rates and suggests that cells and molecules other than RBCs have little effect on the viscosity, at least under healthy conditions. The LD-RBC model underestimates somewhat the experimental data, but is generally in good agreement over the whole range of shear rates, and again demonstrates the effect of aggregation. The agreement is remarkable in view of the simplicity and economy of that model. Errors in simulated viscosities shown in Fig. 1*A* are approximately 30% for the shear rate $\dot{\gamma} = 0.014$ s^{-1} and decrease rapidly with the increase of $\dot{\gamma}$, becoming about 1–3% at high shear rates.

The dependence of whole blood and ES viscosity on hematocrit is demonstrated in Fig. 1*B*. The curves are measured viscosities as a function of H at constant shear rate by Chien et al. (2), and the points are calculated with the LD-RBC model. The plot clearly shows how the latter captures the (hematocrit) H dependence on viscosity, and that the model again demonstrates aggregation to be crucial for a quantitative account of the difference between the viscosity of whole blood and that of washed ES. Recent attempts in modeling (24, 25) of two-cell and multiple-cell aggregates (17) simulated only their flow behavior. Specifically, in ref. 17, the link of viscosity to RBC aggregation was investigated, but the viscosity predictions failed to capture the steep rise of that function at low shear rates.

Reversible Rouleaux Formation. The formation of rouleaux in blood occurs in equilibrium and at sufficiently small shear rates, whereas large shear rates result in immediate dispersion of fragile RBC structures. Experimentally, aggregation is observed (1, 4, 26) to be a two-step process: the formation of a few RBCs into short linear stacks, followed by their coalescence into long linear and branched rouleaux. As the shear rate increases, the large rouleaux break up into smaller ones, and at higher values, the suspension ultimately becomes one of monodispersed RBCs (27). This process then reverses as the shear rate is decreased.

This typical formation–destruction behavior of rouleaux is consistent with the results of our simulations using both the LD-RBC and the MS-RBC models as shown in Fig. 2 (see *SI Text*). At low shear rates (left frames), the initially dispersed RBCs aggregate into large rouleaux of up to about 20 RBCs; as the shear rate is increased to moderate values (middle frames), these structures are reduced in size until at high rates (right frames) they are dispersed almost completely into individual RBCs. Reversibility is demonstrated by reduction of the shear rate to the formation value, at which point individual RBCs begin to reaggregate.

Yield Stress and Aggregation. Whole blood is believed to exhibit a yield stress (i.e., a threshold stress for flow to begin) (1, 10, 11), but this has been difficult to confirm experimentally or theoretically. The most reproducible yield stresses for whole blood are those extrapolated to zero shear rate from viscometric data on the basis of Casson's equation given by (28)

$$\tau_{xy}^{1/2} = \tau_y^{1/2} + \eta^{1/2}\dot{\gamma}^{1/2}, \qquad [1]$$

where τ_y is a yield stress and η is the suspension viscosity at large $\dot{\gamma}$. Note that when the yield stress τ_y vanishes, Eq. **1** reduces to the Newtonian liquid. The assumptions of Casson's relation appear to hold at least at low shear rates, which was successfully demonstrated for pigment-oil suspensions (28), Chinese ovary hamster

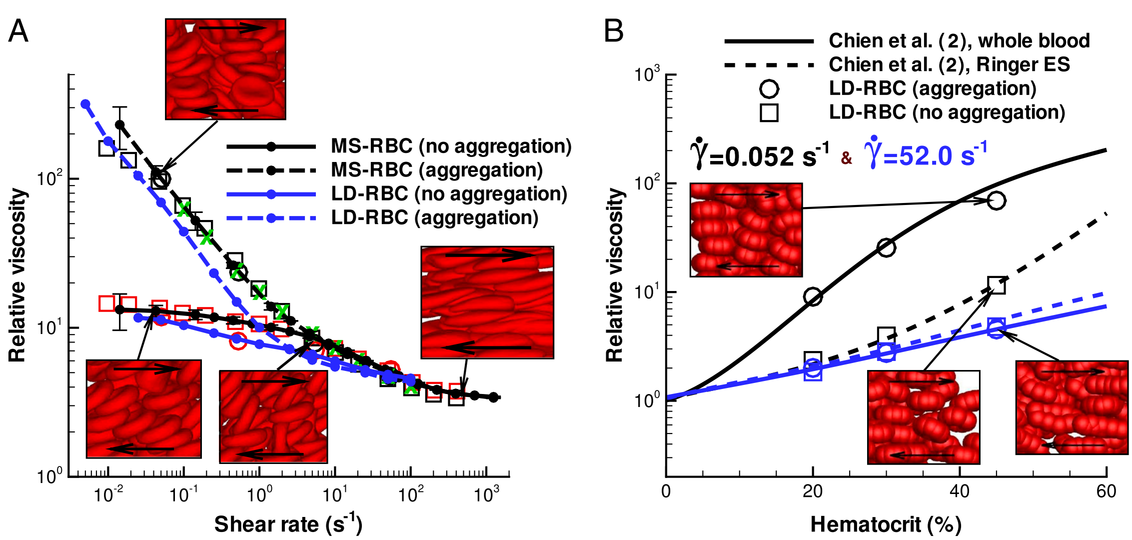

Fig. 1. Validation of simulation results for whole blood and Ringer ES. (*A*) Plot of non-Newtonian relative viscosity (the cell suspension viscosity normalized by the solvent viscosity) as a function of shear rate at $H = 45\%$ and 37 °C. Simulated curves of this work, as indicated and experimental points as follows: Whole blood: green crosses, Merril et al. (1); black circles, Chien et al. (2; black squares, Skalak et al. (3). Ringer ES: red circles, Chien et al. (2); red squares, Skalak et al. (3). Error bars on the MS-RBC viscosity curves reflect one standard deviation and each point on the simulated curves corresponds to a single simulation. (*B*) Plot of relative viscosity as a function of hematocrit (H) at shear rates 0.052 (black) and 5.20 (blue) s^{-1}: simulated (LD-RBC points), and Chien et al. (2) experimental fits for whole blood (solid lines), and Ringer ES (dashed lines).

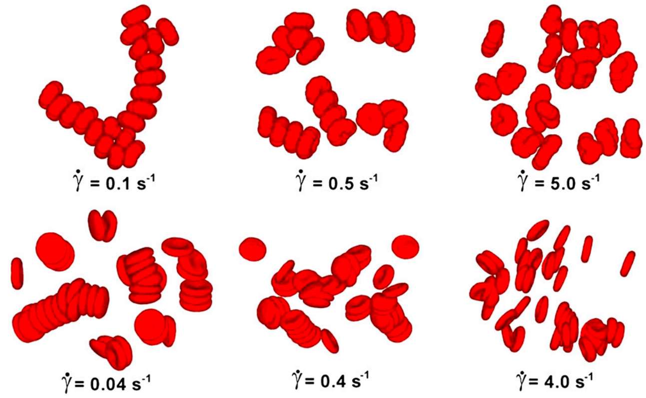

Fig. 2. Visualization of aggregation. Simulated reversible rouleaux are formed by LD-RBC model (*Upper*) and MS-RBC model (*Lower*) with $H = 10\%$. The left column corresponds to low shear rates, center column to moderate share rates, and right column to high shear rates as indicated on the plots; see *SI Text*.

cell suspensions (29), and blood (7). Following the extrapolation method in ref. 7, we fit a polynomial in Casson coordinates ($\dot{\gamma}^{1/2}$, $\tau_{xy}^{1/2}$) to the simulated data for a $H = 45\%$ suspension shown in Fig. 3*A*. The fitting clearly indicates the extrapolated τ_y to be nonzero for the aggregating RBC suspension and zero without cell aggregation.

The yield stress for blood has previously been attributed to the presence of rouleaux in experiments reported in refs. 1, 10 and 11. In practice, the measurement of yield stress is complicated by the nature of suspension and type of instrument used (30). As an example, at the lowest shear rates sedimentation and viscometer wall effects are complicating factors, and yield stresses derived from viscometric data are not consistent with those derived from nonrheological measurements (6). Merrill et al. (1) found τ_y of healthy human blood to lie between 0.0015 and 0.005 Pa at $H = 45\%$, and to vary as $H^{1/3}$, similar to the dependence Thurston (31) described for the elastic modulus of blood. Copley et al. (11) measured blood properties at very low shear rates down to 0.001 s^{-1}, and still found evidence for a yield stress. Fig. 3*B* shows that the simulated τ_y obtained by the extrapolation in Casson coordinates are in good agreement with viscometric data, consistent with the agreement between the computed and the measured viscosities.

Micro-to-Macro Link. The non-Newtonian nature of blood (e.g., shear thinning, yield stress) emerges from the interactions between cells and from their properties and dynamics. Therefore, we examined the structure and dynamics of the modeled suspensions on the level of single cells. We found null pair correlations of RBC *centers of mass* for each direction (x,y,z), which indicates that the cell suspensions do not self-assemble or order themselves in any direction at $H = 45\%$. This finding contradicts with suspensions of spherical colloids, which have been shown (32) to self-assemble near the close-packing concentration. To examine the cell suspension's local microstructure, we calculate the radial distribution function (RDF) of RBC centers shown in Fig. 4*A*. An equivalent isotropic structure factor can be found in *SI Text*. For the no-aggregation case, we find that no significant structures formed over the entire range of shear rates. At the lowest shear rate (red solid line), several small peaks in RDF indicate the presence of infrequent intermediate structures because RBCs may have enough time to relax locally at very low shear rates. A larger peak of the red solid curve at $r = 8$ μm, which is equal to the cell diameter, indicates that neighboring RBCs are often aligned with each other in the flow. As seen from the other solid curves (blue, green, and black), the correlations completely disappear at higher shear rates, and therefore the shear thinning behavior of a non-aggregating suspension is clearly not due to a change in microstructure. In contrast, several large peaks in the RDF function for the aggregating case at the lowest shear rate $\dot{\gamma} = 0.045$ s^{-1} (red dashed line) indicate the formation of rouleaux of two to four RBCs. An increase of the shear rate leads to the dispersion of rouleaux shown by the blue dashed curve in Fig. 4*A*, where predominant RBC aggregates are formed by only two RBCs. At shear rates above approximately 5–10 s^{-1}, no difference in microstructure is detected between aggregating and nonaggregating cell suspensions. As a conclusion, the steep increase in viscosity of the aggregating blood at low shear rates is mainly due to the cell aggregation into rouleaux. In addition, rouleaux formation also provides a plausible explanation for the existence of yield stress, because with decrease of shear rate, larger rouleaux structures are formed resulting in an eventual "solidification" of the suspension.

The dynamics of a single RBC in shear flow is characterized by the tumbling motion at low shear rates and membrane tank-treading at high shear rates (13–15). The tumbling-to-tank-treading transition occurs within a certain range of intermediate shear rates, where an RBC may experience high bending deformations

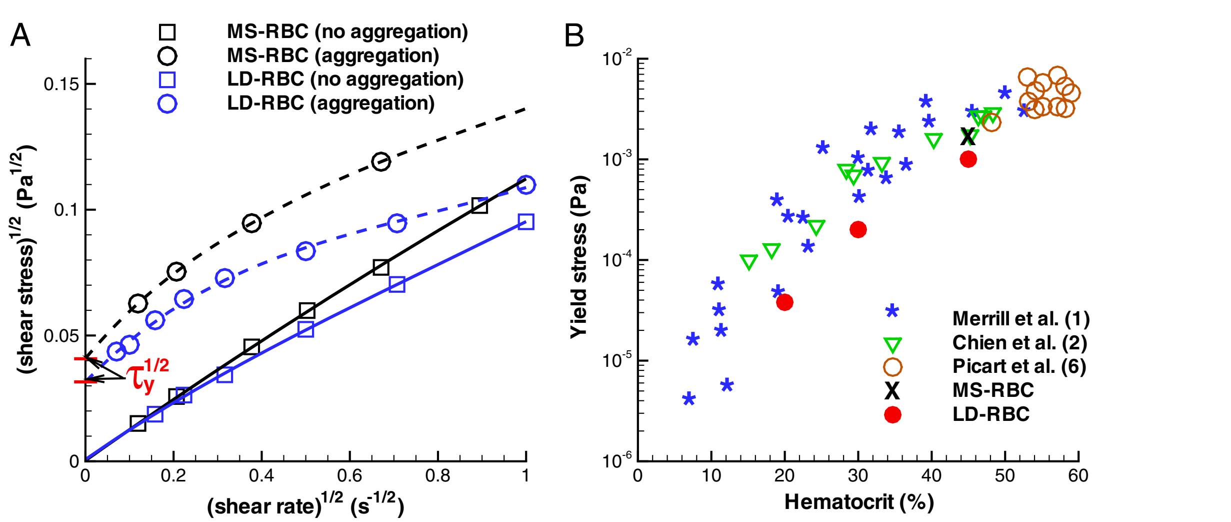

Fig. 3. Correlation of aggregation with yield stress. (*A*) Casson plots with a polynomial fit showing the extrapolated intercept τ_y for simulated MS-RBC and LD-RBC suspensions with (dashed lines) and without (solid lines) aggregation at $H = 45\%$. (*B*) Yield stress as a function of hematocrit H for simulated suspensions with aggregation compared with experimental values derived from viscosity measurements: blue stars, Merril et al. (1); green triangles, Chien et al. (2); open circles, Picart et al. (6).

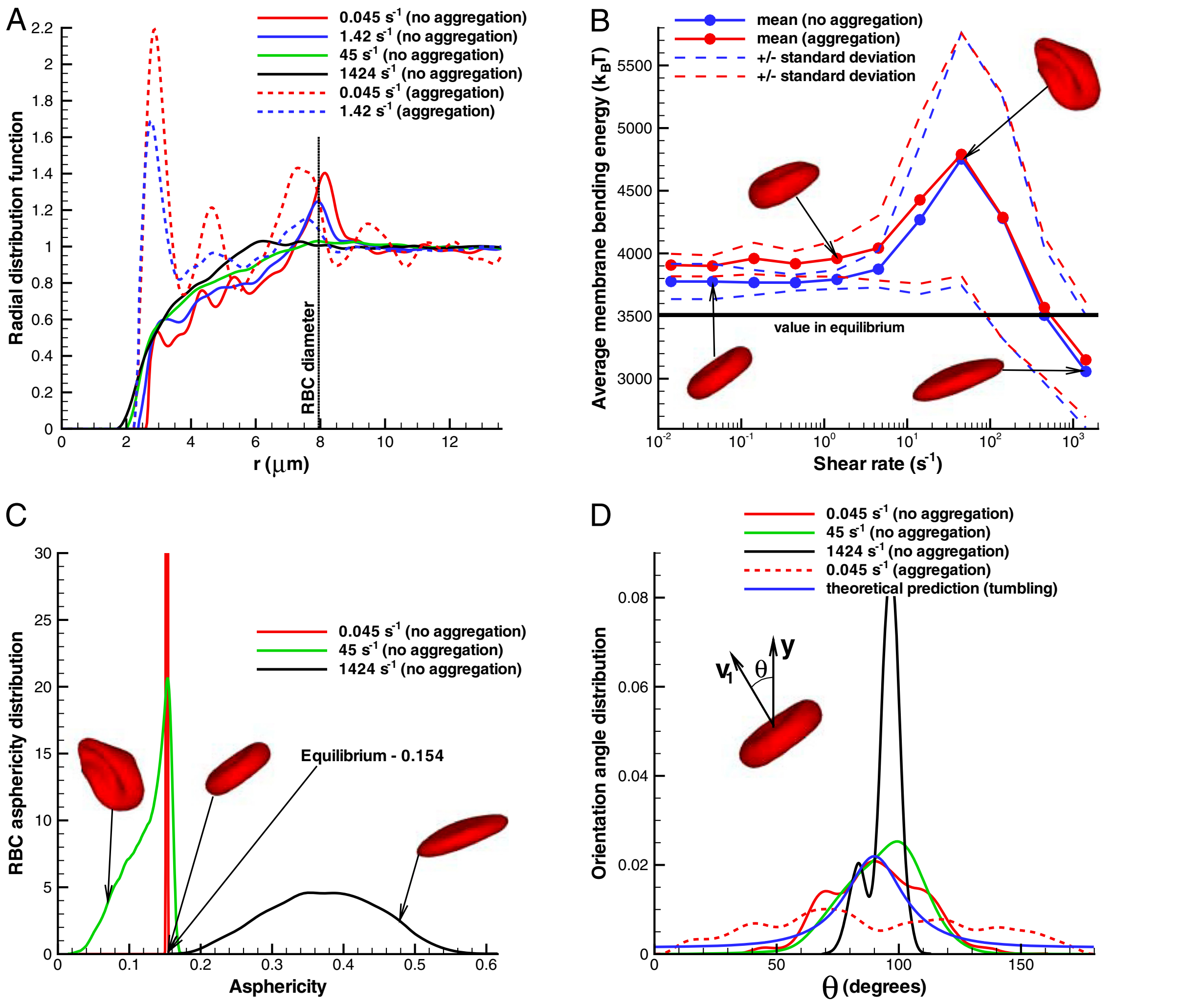

Fig. 4. Structural and dynamical properties of RBC suspensions with $H = 45\%$ for the MS-RBC model. Snapshots show sample RBC conformations from simulations. (*A*) Radial distribution function showing cell suspension's structure. (*B*) Average membrane bending energy with respect to shear rate showing correlation between single-cell deformation and dynamics. Dashed lines are the corresponding mean values ±1 SD. (*C*) RBC asphericity distributions characterizing the deviation from a spherical shape as a function of shear rate. The asphericity is defined as $[(\lambda_1 - \lambda_2)^2 + (\lambda_2 - \lambda_3)^2 + (\lambda_3 - \lambda_1)^2]/(2R_g^4)$, where $\lambda_1 \le \lambda_2 \le \lambda_3$ are the eigenvalues of the gyration tensor and $R_g^2 = \lambda_1 + \lambda_2 + \lambda_3$. The asphericity for a single RBC in equilibrium is equal to 0.154. (*D*) Orientational angle distributions for various shear rates that illustrate single-cell dynamics. The cell orientational angle is given by the angle between the eigenvector V_1 of the gyration tensor and the flow-gradient direction (*y*). Theoretical prediction showing the orientational angle distribution of a single tumbling RBC in shear flow is calculated from the theory in ref. 13.

(15). The deformation, orientation, and dynamics of cells within the suspension is illustrated in Fig. 4 *B–D*. These plots show that cells in the suspension mostly tumble and retain their biconcave shape at low shear rates below 5 s^{-1}, which is confirmed by essentially no change in RBC bending energy and in its standard deviation (Fig. 4*B*), by the extremely narrow asphericity distribution around the equilibrium value of 0.154 (Fig. 4*C*), and by the wide orientational angle (θ) distribution in Fig. 4*D*. Cell tumbling at low shear rates is slightly hindered in nonaggregating suspensions in comparison to tumbling of a single RBC in shear flow due to cell crowding, which results in sliding of cells over each other; this is shown by a higher peak in the orientational angle distribution (green curve) in Fig. 4*D* with respect to the theoretical prediction (blue curve). In contrast, RBC tumbling in aggregating suspensions appears to be nearly uniform because RBCs tumble within multiple-cell rouleaux structures. At high shear rates, larger than about 200 s^{-1}, individual RBCs are subject to tank-treading motion illustrated by a narrow θ distribution (black line) in Fig. 4*D*. At yet higher shear rates, RBCs become strongly elongated as indicated by the RBC asphericity distribution in Fig. 4*C*.

The most interesting and complex cell dynamics, however, occurs in the broad intermediate regime of shear rates between 5 and 200 s^{-1}, where RBC aggregation interactions can be neglected. This range also corresponds to the main region of shear thinning for the nonaggregating cell suspension. In this range of shear rates, RBCs within the suspension experience severe deformations documented by a pronounced increase in the membrane bending energy and in its variation shown in Fig. 4*B*. The asphericity distribution for $\dot{\gamma} = 45$ s^{-1} in Fig. 4*C* shows that RBCs attain on average a more spherical shape, indicating transient folded conformations. These deformations may result in a reduction of shear stresses due to collisional constraints of cell tumbling, and therefore in shear thinning. In addition, the transition of some cells to the tank-treading motion further reduces the shear stresses contributing to the viscosity thinning.

Tunable Properties of Cell Suspensions. The computational framework presented herein is general and can be employed to investigate other cell, vesicle, and capsule suspensions with potential usage in biology, medicine, and engineering. The suspension properties may be tuned to yield a desired behavior by changing

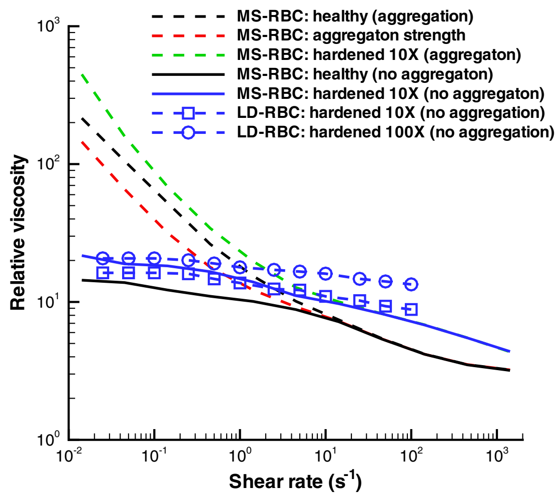

Fig. 5. Tunable properties of cell suspensions. MS-RBC and LD-RBC models with $H = 45\%$. Black lines are viscosities of healthy blood with and without aggregation by MS-RBC. Red line illustrates a decrease in cell aggregation strength reduced twice. Blue and green lines represent the viscosities of hardened RBC suspensions with 10× (MS-RBC and LD-RBC) and 100× (LD-RBC) higher Young's modulus than that in health. Each point on the simulated curves corresponds to a single simulation.

the solvent viscosity, material properties of suspended cells, and intercell aggregation interactions. Fig. 5 shows several examples of the tunable properties of cell suspensions. Results for cells with 10 and 100 times higher Young's modulus than healthy RBCs (blue and green curves) show a considerable increase of viscosity. Hardened RBCs are known (33, 34) to increase their suspension viscosities, and they are highly relevant in many hematologic disorders and diseases, e.g., malaria, sickle-cell anemia, spherocytosis. In addition, aggregating suspensions of stiffer cells show a steeper rise in viscosity at low shear rates resulting in a substantially higher yield stress. Fig. 5 also illustrates the expected decrease, relative to whole blood, in the suspension viscosity at low shear rates (red curve) due to a twofold reduction in the aggregation strength (D_e, see *Methods*). The significant change in viscosity observed above implies a strong dependence of flow properties on cell deformability and adhesive cell interactions.

Magnitude of Aggregation Forces. The predictions of Fig. 1 show that a suspension of modeled RBCs captures the viscosity of healthy whole blood with cell aggregation. The plausibility of the aggregation strength was checked by calculation of the maximum force needed to break up two aggregated RBCs (see *SI Text*). The breakup pulling force in the normal direction is about 3.0–7 pN, where the lower value corresponds to a peeling breakup. Tangential or sliding breakup requires a force in the range of 1.5–3 pN. These forces are much smaller than those imposed on single RBCs in stretching tests with optical tweezers (35), and they are consistent with observations of rouleaux, which do not show any large cell deformations. In addition, measurements of a disaggregation force in shear flow by Chien et al. (36) indicate that the shear stress required to break up a rouleaux structure lies approximately between 0.01 and 0.1 Pa, whereas the analogous simulations with the MS-RBC model yield about 0.02 Pa (see *SI Text*).

Conclusions. The accurate prediction of the non-Newtonian behavior from simulations of cell suspensions suggests a new paradigm for rheology of cell suspensions and blood in particular. As an example, an abnormal increase in RBC aggregation is a pathological state associated with many diseases, such as deep venous thrombosis, atherosclerosis, AIDS, myeloma, and diabetes mellitus, which may afflict many different sites of the human arterial tree (37–40). However, such correlations have had few theoretical guidelines for their interpretation. The modeling of cells whose parameters are determined from experiments on single cells (41) can be extended to abnormal and diseased cells, and in combination with the aggregation model, their suspensions can be simulated to allow quantitative comparison with rheological measurements and to guide in vivo ultrasonic measurements to yield a more precise diagnosis of the aforementioned diseases (40). The predictive capability of accurate modeling of cell and capsule suspensions can be readily extended to a variety of engineering and material science applications. Such simulations may aid in the development of new soft materials and may drive the tuning process and optimization of their properties.

Methods

Simulation Method. The DPD method (20, 21) is a particle-based mesoscopic simulation technique. A DPD system is represented by N point particles, which interact through pairwise soft potentials and move according to the Newton's second law of motion; see also *SI Text*.

RBC Models. An MS-RBC (15) is constructed by a collection of discrete points (500 in this work), which are the vertices of a triangular network of springs with a "dashpot" on the membrane surface. The network assumes fixed connectivity and supplies the elastic and the viscous response of an RBC membrane. To mimic membrane bending rigidity, a bending resistance is implemented between all neighboring triangular plaquettes. In addition, area and volume constraints are enforced to model incompressibility of an RBC membrane and the cytosol, respectively. The LD-RBC model (23) is constructed as a closed torus-like ring of 10 overlapping colloidal particles connected by springs. Each colloidal particle is represented by a single DPD particle with a repulsive core. A bending resistance between two neighboring springs is also incorporated. More details on the RBC models can be found in the *SI Text*.

Aggregation Models. For a blood suspension, the attractive cell–cell interactions are crucial for simulation of aggregation into rouleaux. These forces are approximated using the Morse potential $U(r) = D_e[e^{2\beta(r_0-r)} - 2e^{\beta(r_0-r)}]$, where r is the separation distance, r_0 is the zero force distance, D_e is the well depth of the potential, and β characterizes the interaction range. For the MS-RBC model, the Morse potential interactions are implemented between every pair of vertices of separate RBCs if they lie within a defined potential cutoff radius. For the LD-RBC model, the aggregation force acts between centers of mass of different RBCs if the cells are properly aligned. Thus, the Morse potential is applied only if the angle between the normals of two cells does not exceed a critical angle. The aggregation forces for blood were calibrated for a single shear rate and no further adjustments were made in the subsequent computation of suspension viscosity. More details on the aggregation models can be found in the *SI Text*.

ACKNOWLEDGMENTS. This work was supported by National Institutes of Health Grant R01HL094270 and simulations were performed on the Cray XT5 at the National Science Foundation–National Institute for Computational Science and at the Jülich Supercomputing Center in Germany.

1. Merrill EW, et al. (1963) Rheology of human blood near and at zero flow. *Biophys J* 3:199–213.
2. Chien S, Usami S, Taylor HM, Lundberg JL, Gregersen MI (1966) Effects of hematocrit and plasma proteins on human blood rheology at low shear rates. *J Appl Physiol* 21:81–87.
3. Skalak R, Keller SR, Secomb TW (1981) Mechanics of blood flow. *J Biomech Eng* 103:102–115.
4. Schmid-Schönbein H, Wells RE (1971) Rheological properties of human erythrocytes and their influence upon the "anomalous" viscosity of blood. *Ergeb Physiol Biol Chem Exp Pharmakol* 63:146–219.
5. Thurston GB (1996) *Advances in Hemodynamics and Hemorheology*, ed TV How (JAI Press, Greenwich, CT), pp 1–30.
6. Picart C, Piau JM, Galliard H (1998) Human blood shear yield stress and its hematocrit dependence. *J Rheol* 42:1–12.

7. Merrill EW, Gilliland ER, Lee TS, Salzman EW (1966) Blood rheology: Effect of fibrinogen deduced by addition. *Circ Res* 18:437–446.
8. Chien S, et al. (1967) Blood viscosity: Influence of erythrocyte aggregation. *Science* 157:829–831.
9. Chien S, Usami S, Kellenback RJ, Gregersen MI (1970) Shear-dependent interaction of plasma proteins with erythrocytes in blood rheology. *Am J Physiol* 219:143–153.
10. Cokelet G, et al. (1963) The rheology of human blood—measurement near and at zero shear rate. *Trans Soc Rheol* 7:303–317.
11. Copley AL, Huang CR, King RG (1973) Rheogoniometric studies of whole human blood at shear rates from 1000 to 0.0009 sec^{-1}. I. Experimental findings. *Biorheology* 10:17–22.
12. Noguchi H, Gompper G (2005) Shape transitions of fluid vesicles and red blood cells in capillary flows. *Proc Natl Acad Sci USA* 102:14159–14164.
13. Abkarian M, Faivre M, Viallat A (2007) Swinging of red blood cells under shear flow. *Phys Rev Lett* 98:188302.
14. Pivkin IV, Karniadakis GE (2008) Accurate coarse-grained modeling of red blood cells. *Phys Rev Lett* 101:118105.
15. Fedosov DA, Caswell B, Karniadakis GE (2010) A multiscale red blood cell model with accurate mechanics, rheology, and dynamics. *Biophys J* 98:2215–2225.
16. Pozrikidis C (2010) *Computational Hydrodynamics of Capsules and Biological Cells*, ed C Pozrikidis (CRC, Boca Raton, FL).
17. Liu Y, Liu WK (2006) Rheology of red blood cell aggregation by computer simulation. *J Comput Phys* 220:139–154.
18. McWhirter JL, Noguchi H, Gompper G (2009) Flow-induced clustering and alignment of vesicles and red blood cells in microcapillaries. *Proc Natl Acad Sci USA* 106:6039–6043.
19. Fedosov DA, Caswell B, Suresh S, Karniadakis GE (2010) Quantifying the biophysical characteristics of *Plasmodium-falciparum*-parasitized red blood cells in microcirculation. *Proc Natl Acad Sci USA* 108:35–39.
20. Hoogerbrugge PJ, Koelman JMVA (1992) Simulating microscopic hydrodynamic phenomena with dissipative particle dynamics. *Europhys Lett* 19:155–160.
21. Espanol P, Warren P (1995) Statistical mechanics of dissipative particle dynamics. *Europhys Lett* 30:191–196.
22. Noguchi H, Gompper G (2004) Fluid vesicles with viscous membranes in shear flow. *Phys Rev Lett* 93:258102.
23. Pan W, Caswell B, Karniadakis GE (2010) A low-dimensional model for the red blood cell. *Soft Matter* 6:4366–4376.
24. Bagchi P, Popel AS, Johnson PC (2005) Computational fluid dynamic simulation of aggregation of deformable cells in a shear flow. *J Biomech Eng* 127:1070–1080.
25. Wang T, Pan TW, Xing ZW, Glowinski R (2009) Numerical simulation of rheology of red blood cell rouleaux in microchannels. *Phys Rev E Stat Nonlin Soft Matter Phys* 79:041916.
26. Samsel RW, Perelson AS (1982) Kinetics of rouleau formation: I. A mass action approach with geometric features. *Biophys J* 37:493–514.
27. Zhao Q, Durand LG, Allard L, Cloutier G (1998) Effects of a sudden flow reduction on red blood cell rouleau formation and orientation using RF backscattered power. *Ultrasound Med Biol* 24:503–511.
28. Casson N (1992) *Rheology of Disperse Systems*, ed CC Mill (Pergamon, New York), pp 84–104.
29. Iordan A, Duperray A, Verdier C (2008) Fractal approach to the rheology of concentrated suspensions. *Phys Rev E Stat Nonlin Soft Matter Phys* 77:011911.
30. Meiselman HJ (1980) *Erythrocyte Mechanics and Blood Flow*, eds GR Cokelet, HJ Meiselman, and DE Brooks (Liss, New York), pp 75–117.
31. Thurston GB (1972) Viscoelasticity of human blood. *Biophys J* 12:1205–1217.
32. Pan W, Caswell B, Karniadakis GE (2010) Rheology, microstructure and migration in Brownian colloidal suspensions. *Langmuir* 26:133–142.
33. Chien S, Usami S, Dellenback RJ, Gregersen MI (1967) Blood viscosity: Influence of erythrocyte deformation. *Science* 157:827–829.
34. Brooks DE, Goodwin JW, Seaman GV (1970) Interactions among erythrocytes under shear. *J Appl Physiol* 28:172–177.
35. Suresh S, et al. (2005) Connections between single-cell biomechanics and human disease states: Gastrointestinal cancer and malaria. *Acta Biomater* 1:15–30.
36. Chien S, Sung LA, Kim S, Burke AM, Usami S (1977) Determination of aggregation force in rouleaux by fluid mechanical technique. *Microvasc Res* 13:327–333.
37. Dintenfass L (1980) Molecular rheology of human blood: Its role in health and disease (today and tomorrow). *Proc 8th Int Cong Rheol (Naples)*, eds G Astarita, G Marrucci, and L Nicilais 3 (Springer, New York), pp 467–480.
38. Lowe GDO (1998) *Clinical Blood Rheology*, (CRC, Boca Raton, FL), 1–2.
39. Robertson AM, Sequeira A, Kameneva MV (2008) Hemodynamical flows. *Modeling, Analysis and Simulation)*, 37 (Birkhauser, Basel), pp 63–120.
40. Franceschini E, et al. (2010) Ultrasound characterization of red blood cell aggregation with intervening attenuating tissue-mimicking phantoms. *J Acoust Soc Am* 127:1104–1115.
41. Bao G, Suresh S (2003) Cell and molecular mechanics of biological materials. *Nat Mater* 2:715–725.